# Oxidation and crystallization behavior of calcium europium silicon nitride thin films during rapid thermal processing

M. de Jong **(Delft University)**
V.E. van Enter **(Delft University)**
E.W. Schuring **(ECN)**
E. van der Kolk **(Delft University)**

Maart 2015
ECN-W--13-015

**Oxidation and crystallization behavior of calcium europium silicon nitride thin films during rapid thermal processing**

M. de Jong[a,*], V.E. van Enter[a] , E.W. Schuring[b], E. van der Kolk[a]

[*]*Corresponding author. Faculty of Applied Science, Delft University of Technology, Mekelweg 15, 2629JB Delft, The Netherlands. E-mail: m.dejong-1@tudelft.nl, Telephone: 00316152785865. Fax:*

[a]*Faculty of Applied Science, Delft University of Technology, Mekelweg 15, 2629JB Delft, The Netherlands. E-mail: vvanenter@gmail.com, e.vanderkolk@tudelft.nl*

[b]*Energy Center of the Netherlands, Westerduinweg 3, 1755LE Petten, The Netherlands. E-mail: schuring@ecn.nl.*

Highlights:

- A thin film of nitridated Ca, Si and Eu was deposited using magnetron sputtering
- Rapid thermal processing results in $Eu^{2+}$ doped $Ca_3Si_2O_4N_2$, $Ca_2SiO_4$, and $CaSiO_3$
- Oxidation rate differs with position due to radial temperature gradient during RTP
- Cross-section SEM-EDS shows how the oxidation progresses in lateral direction
- A stepwise oxidation process forms $Ca_3Si_2O_4N_2$, then $Ca_2SiO_4$, and finally $CaSiO_3$

[*]Corresponding author. Telephone: 00316152785865. Fax:

Keywords: magnetron sputtering; luminescent thin film; rapid thermal processing; divalent europium; oxidation reaction.

**Abstract**

Luminescent thin films were fabricated on silicon wafers using reactive magnetron sputtering of Ca, Si and Eu in $Ar/N_2$ atmosphere. In order to activate the luminescence, the as-deposited nitride films were heated to 1100$^o$C by a rapid thermal processing (RTP) treatment. X-ray diffraction (XRD) measurements reveal the crystal phases that form during RTP treatment. By recording scanning electron microscopy (SEM) images of the surface and the cross-section of the film at different radial locations, the formation of different layers with a thickness depending on the radial position is revealed. Energy dispersive x-ray spectroscopy (EDX) analysis of these cross-sections reveals the formation of an oxide top layer and a nitride bottom layer. The thickness of the top layer increases as a function of radial position on the substrate and the thickness of the bottom layer decreases accordingly. The observation of different $4f^6 5d^1 \rightarrow 4f^7$ $Eu^{2+}$ luminescence emission bands at different radial positions correspond to divalent Eu doped $Ca_3Si_2O_4N_2$, $Ca_2SiO_4$ and $CaSiO_3$, which is in agreement with the phases identified by XRD analysis. A mechanism for the observed oxidation process of the nitride films is proposed that consists of a stepwise oxidation from the as-deposited amorphous nitride state to crystalline $Ca_3Si_2O_4N_2$, to $Ca_2SiO_4$ and finally $CaSiO_3$. The oxidation rate and final state of oxidation show a strong temperature-time dependency during anneal treatment.

## 1. Introduction

The absorption and emission properties of divalent Eu doped calcium silicon oxide [1-3], oxynitride [4-6] and nitride [7] phosphors make them an interesting class of luminescent materials for application in solid state lighting or afterglow. In addition, luminescent materials could enhance the efficiency of photovoltaic devices considerably when applied as spectral shifting or down-conversion thin films [8-10]. Theoretical calculations indicate that luminescent metal silicon oxides and (oxy)nitrides are interesting classes of materials for this application [11]. A possible approach to applying the luminescent materials is by depositing them as thin films on the surface of a photovoltaic device. In order to do so, a more fundamental understanding is required of the thin film deposition and the oxidation and crystallization processes that take place during high temperature anneal of as-deposited films.

Earlier work has shown that thin films typically show low oxygen content after they are extracted from the sputter system. The oxygen content increases strongly when an RTP anneal treatment is performed [12], indicating that the oxidation process is strongly temperature dependent. In this work the oxidation process of the nitride films is studied in more detail by an ex-situ study of the influence of RTP on the structure, composition and luminescence characteristics of a thin film that is fabricated by reactive magnetron sputtering of Ca, Si and Eu in an Ar/$N_2$ atmosphere.

The thin film deposition process, the anneal treatment and the characterization methods are described in the materials and methods section. In the results section XRD, SEM, EDX analysis and Photoluminescence (PL) data are presented as a function of the radial position on the film. Identification of different stages of the oxidation reaction, is explained in the discussion section. Finally conclusions are presented on the oxidation and crystallization mechanism and the potential of

magnetron sputtering for the formation of luminescent oxide, oxynitride and nitride thin films.

## 2. Experimental details

Thin film deposition was performed with an AJA Orion 5 magnetron sputtering system. Ca (99.5%), Si (99.999%) and Eu (99.99%) were used as sputtering targets. Preparation and installation of the target materials and the sputtering system is done in a special manner when using Ca and Eu sputter targets, as is described in detail in previous work [12].

First the deposition rates of the targets were roughly estimated based on thickness profiling measurements of $SiN_x$, $EuN_x$ and $Ca_xSi_yN_z$ thin films deposited on objective glass, using a range of sputter powers for RF sputtered Ca (25-75 W) and Si (50-150 W) and DC sputtered Eu (10-25 W). Since the density of the sputtered films is unknown, these measurements only give a rough estimation of the molar ratio of deposited atoms. Therefore the molar ratio of Ca to Si and Ca to Eu at different sputter powers were calibrated with EDX measurements on the films.

Using the calibrated relations between molar ratios of sputtered materials and different sputter powers, a thin film was deposited on a rotating 5.1 cm round c-Si (111) substrate. The ratio of deposited Ca to Si was calculated to be 1:1. The Eu target was sputtered in order to have an Ca:Eu ratio of 20:1 in the film. This was achieved by sputtering the Ca, Si and Eu targets simultaneously at 75 W, 150 W and 15 W respectively. The resulting film thickness was calculated at 600 nm.

Since Eu sputter rates are typically much higher than those of Ca and Si, the sputter rate of Eu was decreased 10 times by placing a stainless steel cover disc with equally spaced 1 mm diameter holes on top of the chimney of the sputter gun. The sputter rate was checked by sputtering Eu in an Ar atmosphere on a quartz crystal microbalance (QCM) with and without the cover disc. Due to rapid oxidation of Eu thin films in air, this measurement could not be confirmed by profiling measurements. However, the QCM is considered an adequate technique for measuring relative changes in deposition rates.

In order to crystallize the $CaN_x$, $SiN_x$ and $EuN_x$ materials that are mixed in the as-deposited film, a post-deposition anneal treatment was performed. This was done using a Solaris 150 double-sided illumination RTP system at 1100$^{o}$C with a ramp rate of 40$^{o}$C $s^{-1}$ while flushing with 6 SLM nitrogen gas containing 7% $H_2$. The temperature was measured by placing the back of the substrate on a c-Si thermocouple. The effect of the RTP process on the film was systematically investigated as a function of time during 75 minutes in steps of 5 minutes. In between heat treatments, the film was removed from the RTP and photographed under UV illumination between 340 and 360 nm.

XRD measurements were performed at several radial positions by cutting 5-10 $mm^2$ diameter pieces containing only the desired areas of the thin film. The pieces were glued on 50 mm diameter c-Si (111) wafers in order to properly align the samples in the Panalytical X'pert Pro MRD system. The incident beam angle was fixed at 19.28$^{o}$. 1E16 and 2F2 CSH slits  were used, resulting in an x-ray beam with 1 mm beam height and 2 mm beam width. Grazing incidence diffraction was performed with a

parallel beam geometry. Cu-Kα radiation was used, with U = 40 kV and I = 40 mA. Diffraction patterns were recorded between $20^{o}$ and $70^{o}$ $2\theta$. The step size was $0.02^{o}$ with a step time of 15 s.

The PL measurements were performed after anneal treatment using an optical fiber connected to an Ocean Optics QE65000 spectrometer. The film was excited at a wavelength of 280 nm by using the third harmonic of a 120 fs Ti:sapphire laser.

A HITACHI SU70 Shottky Emission Scanning Electron Microscope with Oxford Aztec EDX-EBSD analyses system and a 50 mm EDX detector was used to record SEM images and measure the elemental composition and distribution with EDX both at 5 kV. The penetration depth of the electron beam is limited to 400 nm at this acceleration voltage as established by Monte Carlo simulations of the mean electron path inside the film. Since the film thickness is calculated at 600 nm, EDX analyses obtained from the surface originate from the thin film only.

It is generally accepted that EDX analyses is limited to qualitative results for O and N, due to physical limitations. This results in a ±5weight% error in the measured O and N, provided that a flat sample is used at the correct working distance (both conditions are satisfied in this investigation). For Ca, Si and Eu, a variance typically not higher than ± 0.5weight% is assumed. Operating parameters, acceleration voltage and beam current were all constant during data acquisition at different positions. This enables for a qualitative comparison of the differences in O and N concentrations as long as they differ more than ±5wt%.

Cross-sections of the film were also measured with SEM and EDX, by milling the side of the cut film for 1.5 hours using an Hitachi IM4000. $Ar^+$ Ions are used for milling of the cross sections to prepare a 1-2 mm sample area width for imaging. The sample temperature is limited to 80°C, hence no effect on element distribution is considered to occur. X-ray mappings are made of the cross sections, resulting in a qualitative indication of the element distribution in the different layers. Taking into account that the spatial resolution for EDX mapping lies between 200-400 nm.

## 3. Results

A luminescent circular pattern first appears at the edge of the c-Si wafer as shown in Fig. 1a. This is the result of crystallization of the nitride film by oxidation during the RTP process as will be shown later. Figure 1 shows that the crystallization and oxidation process at the edge is faster than in the center of the film which effectively causes the luminescent circular patterns to progress radially inward as a function of annealing time.

A change in emission color is observed at the edge of the film from greenish, to white, to yellow with increased RTP time. Formation of additional luminescent areas closer to the center of the film is also observed. The emission color of some of these areas also changes with increasing RTP times. This is demonstrated with photographs of the film that were taken after 10 (a), 30 (b), 55 (c) and 75 (d) minutes of annealing, shown in Fig. 1a-d.

A scale bar is added to Fig. 1d that is drawn from the center of the substrate to the edge at a distance r = 25 mm. The positions $r_1$ = 0 mm, $r_2$ = 7 mm, $r_3$ = 13 mm and $r_4$ = 23 mm, represent the inner non-luminescent region and radial patterns (2-4) with

distinctly different luminescence colors. These four areas resemble all of the observed luminescent phases.

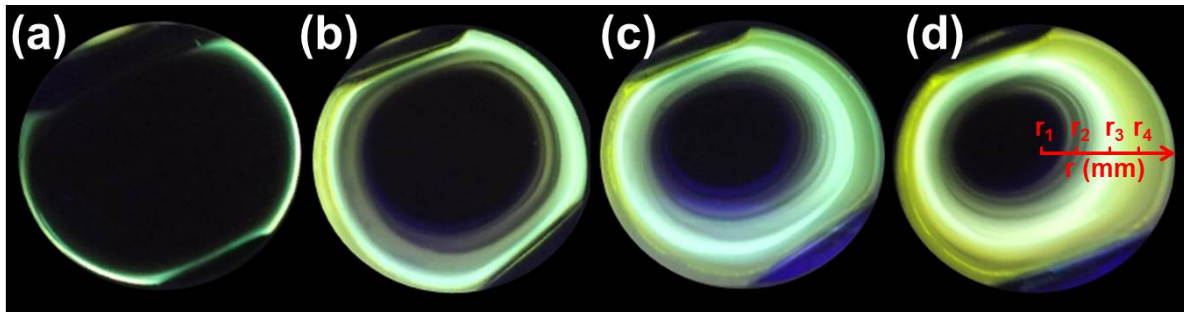


Fig. 1: Photographs of the luminescent thin film under UV illumination after RTP annealing for 10 (a), 30 (b), 55 (c) and 75 (d) minutes. Position numbers 1-4 are at positions $r_1$ = 0 mm, $r_2$ = 7 mm, $r_3$ = 13 mm and $r_4$ = 23 mm respectively.

XRD measurements were performed on positions $r_1$-$r_4$. The results are found in Fig. 2. The intensities of the XRD peaks in the non-luminescent part of the film ($r_1$) is weak but matches $Ca_3Si_2O_4N_2$ (JCPDS code 080-6316). The single high intensity peak observed at 38$^o$ originates from the (111) plane of a $SiO_2$ phase.

At position $r_2$, more diffraction peaks are observed that all match the $Ca_3Si_2O_4N_2$ phase (JCPDS code 080-6316) that was also found at $r_1$. A single peak observed at 28.3$^o$ matches the (111) diffraction line of c-Si.

The diffraction pattern that was measured at $r_3$ shows a diffraction spectrum that could not be matched to a single reference pattern. The majority of the measured peaks (of which the highest intensity peaks are found at diffraction angles 32$^o$, 34.1$^o$, 39.3$^o$ and 41.1$^o$) match with $Ca_2SiO_4$ (JCPDS code 016-5569). The two remaining peaks match with $CaSiO_3$ (JCPDS code 027-0088).

The recorded diffraction spectrum at $r_4$ matches that of $CaSiO_3$ (JCPDS code 027-0088). The single high intensity line measured at diffraction angle 33° matches the (111) diffraction line of CaO (JCPDS code 013-1936).

It can be concluded that when going from the center of the film to the edge an amorphous calcium silicon nitride phase ($r_1$), a crystalline $Ca_3Si_2O_4N_2$ phase ($r_2$), a crystalline $Ca_2SiO_4$ phase ($r_3$) and finally a crystalline $CaSiO_3$ phase ($r_4$) are formed.

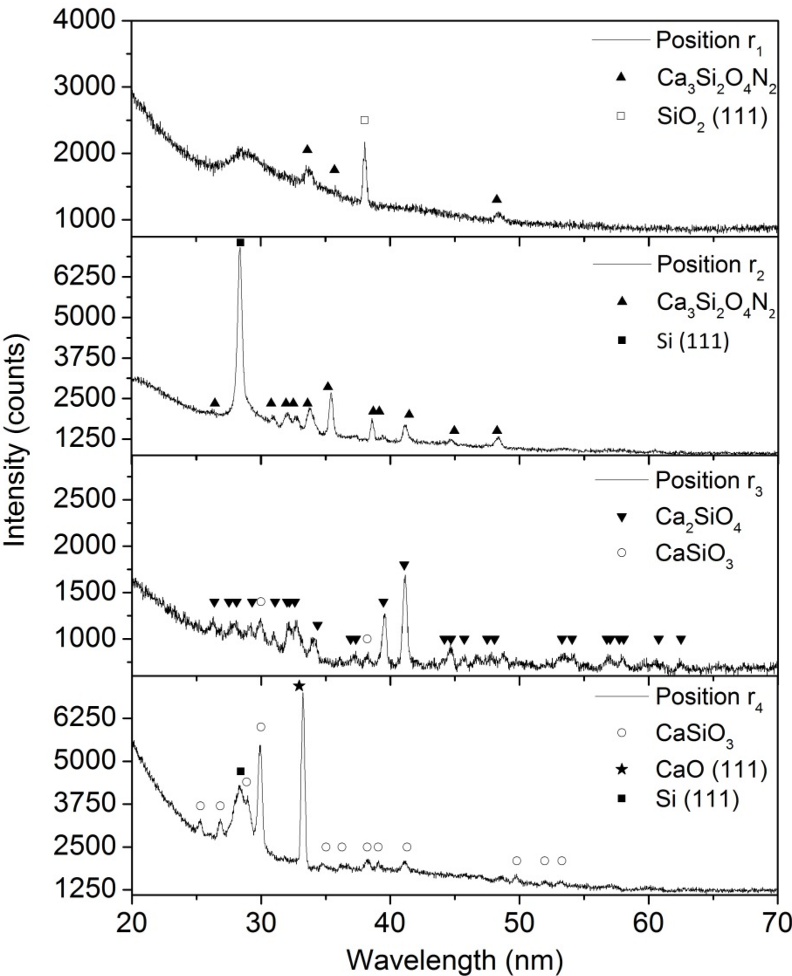


Fig. 2: XRD measurements at positions $r_1$-$r_4$ after 75 min RTP annealing. The symbols in the graphs represent diffraction lines that could be matched with reference patterns.

The surface of the film was imaged with SEM at $r_1$-$r_4$ as shown in Fig. 3. The surface of the black area observed at $r_1$ was found to be smooth. Formation of round structures is observed at $r_2$. At $r_3$ bubble-like structures appear that have increased in size and number at $r_4$.

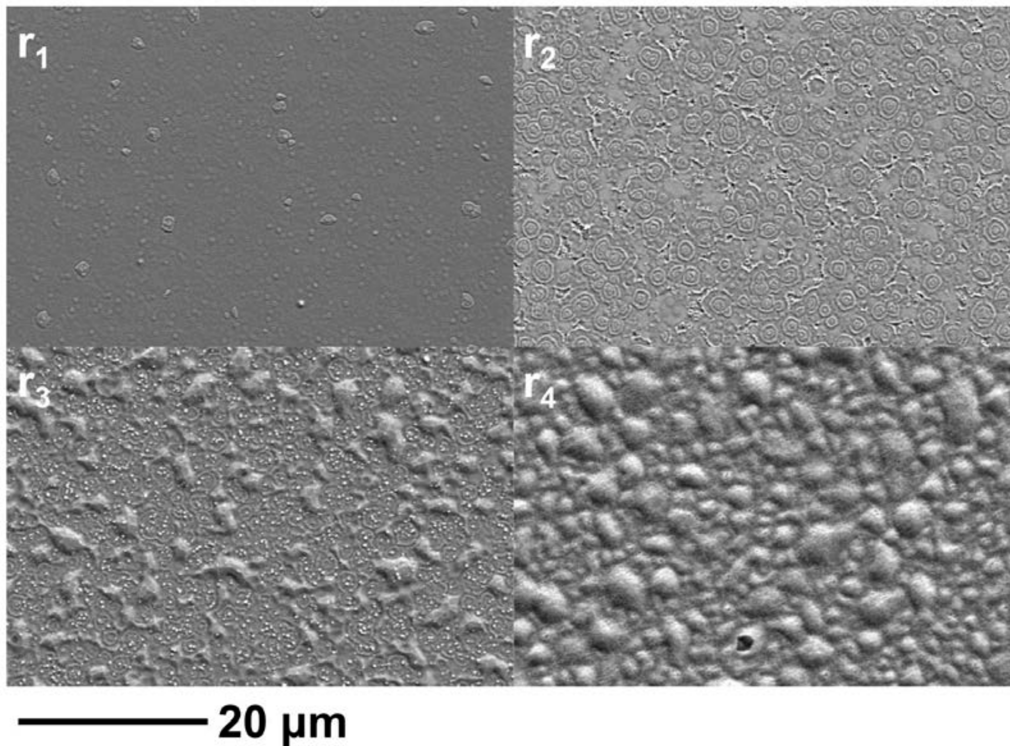


Fig. 3: SEM images of the surface measured at positions $r_1$-$r_4$ after 75min RTP annealing.

EDX measurements were performed along the r-axis in order to study the change in at% ratios from the center to the edge of the film and compare the ratios with the atom ratios in the crystalline phases found with XRD. The results are found in Fig. 4 for the elements Ca, Si, Eu, N and O. The right panel of this figure 4 shows that as-deposited films primarily consist of nitride materials with only a low oxygen content. The left panel shows that the annealed film has an elemental composition that

strongly changes as a function of r, related to differences in temperature as mentioned earlier.

Taking in consideration the 5% variance in the measured N and O wt% as discussed in the experimental section, a clear change in the at% of the two elements is observed with increasing value of r. In the measurement of the as-deposited film, the N at% was found to be significantly higher than the O at%. The highest N content in the annealed film is found in the area where no luminescence is observed, between positions $r_1$ = 0 mm and $r_2$ = 7 mm. The O at% in this area is comparable to the N at%. This indicates that the film is slightly oxidized in the area between $r_1$ = 0 mm and $r_2$ = 7 mm.

A steep increase in the O at% and a corresponding decrease in N at% is observed between $r_2$ = 7 mm and r = 10 mm, which is the transition between the non-luminescent area and the area where the green luminescence is observed. At positions above r = 12 mm no more N signal is observed.

The ratio of the Ca to Si at% is within reasonable agreement with the ratio that was expected from deposition rate measurements. The Eu at% in the film is constant around 1.5 at%. The Ca at% is between 25-30 at%, indicating that the at% ratio of Eu to Ca is approximately 1:20 which is what was anticipated based on the estimated deposition rates of Ca and Eu.

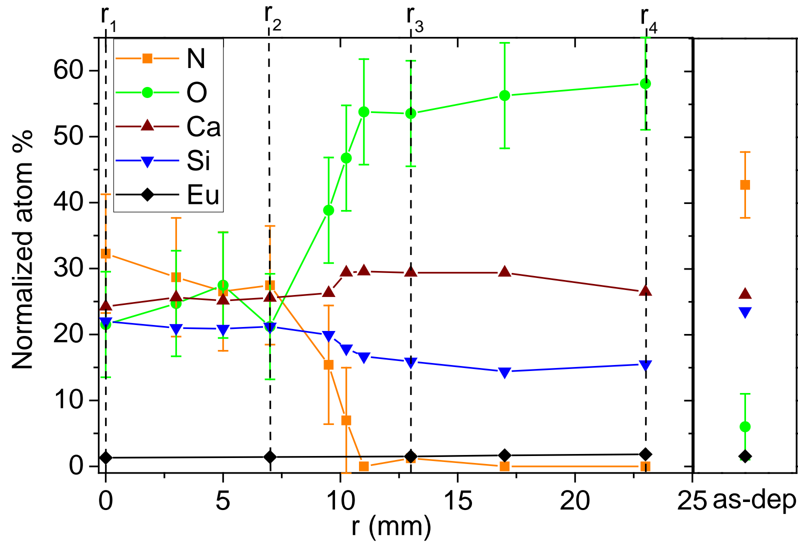


Fig. 4: Plot of the normalized at% of elements present in the thin film ranging from r = 0-23 mm (as defined in Fig. 1d) after 75 minutes of RTP annealing. On the right side of the graph is a measurement of an as-deposited film. The dashed lines indicate measurements performed on the surface of the film at positions $r_1$-$r_4$.

In order to study the elemental composition in the lateral direction, ion-milled cross sections at $r_1$-$r_4$ were prepared and analyzed with SEM and EDX. The results are found in Fig. 5, where an EDX mapping of N and O shows a separation between an oxygen rich top layer and a nitrogen rich bottom layer at each position. When moving from the center to the edge of the film (from $r_1$ to $r_4$), the oxygen containing top layer becomes thicker at the expense of the nitrogen bottom layer that has almost completely disappeared at $r_4$. The thickness of the top layer increases from 100nm ($r_1$), to 600 nm ($r_2$ and $r_3$) to 800 nm ($r_4$). The thickness of the bottom layer decreases from 600nm ($r_1$), to 200 nm ($r_2$ and $r_3$) to 100 nm ($r_4$).

At $r_3$ both a $CaSiO_3$ and $Ca_2SiO_4$ phase were detected with XRD in Fig. 2. The SEM images do not show that there are two different oxide layers present at this position.

This can be explained as the EDX-mapping is less sensitive to differences in composition than EDX-Selected Area (SA) analyses such as the measurements found in Fig. 4. Hence the difference in oxygen content between the two phases is lower than detectable by EDX-mapping. Also the spatial resolution of 200-400 nm at 5 kV impairs the separation between the two phases. Additionally the XRD analyses do not give information on the phase morphology or distribution.

As mentioned earlier the penetration depth for EDX analyses at 5kV is about 400 nm. The total layer is 600 nm and the O-top layer grows towards over 400 nm. Hence, the O- and N-variance as presented in figure 4 will at least partly be related to the growth of the O-layer.

In the EDX mappings no difference in Ca, Si and Eu content was observed between the top layer and the bottom layer. The cracks and open volumes in the top layer confirms the bubble-like structures observed in the SEM images of the surface in Fig. 3c and Fig. 3d.

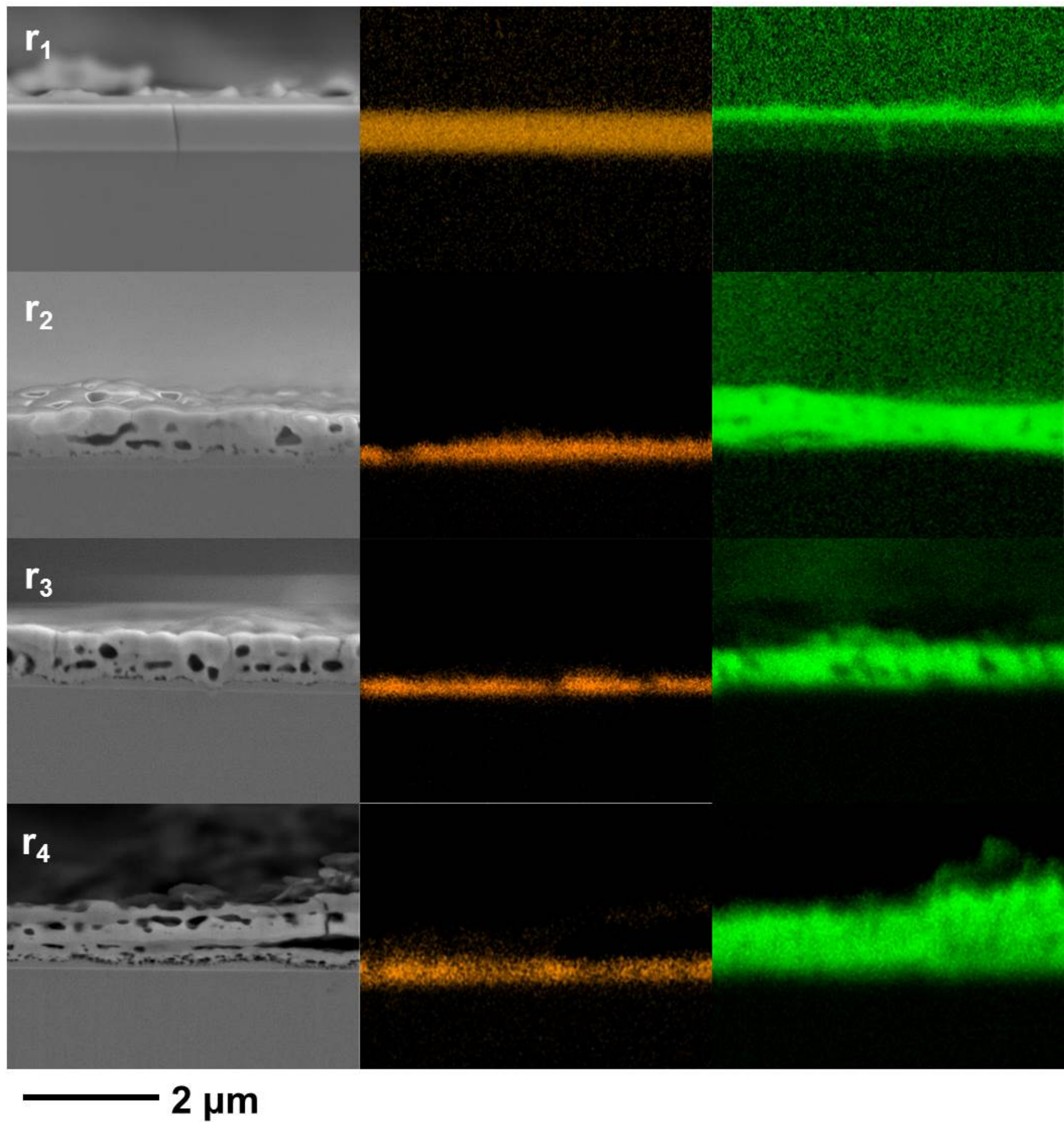


Fig. 5: Cross-section SEM images of the thin film at $r_1$-$r_4$ and the corresponding EDX mappings of N (orange) and O (green) after 75 min RTP treatment

Luminescence emission spectra were recorded at $r_1$-$r_4$, excited at 280 nm by the third harmonic of a femtosecond laser tuned at 840nm. The normalized emission spectra are plotted Fig. 6. No luminescence was observed at $r_1$, which is in accordance with Fig. 1d that also showed no visible luminescence at this position.

The broad emission bands observed at $r_2$-$r_4$ are characteristic for $Eu^{2+}$ $4f^6 5d \rightarrow 4f^7$ transitions. No line emission of $Eu^{3+}$ was observed that is usually found between 600 and 700 nm. This indicates that Eu is incorporated in the crystalline host as $Eu^{2+}$. The presence of multiple emission maxima indicates that there are multiple crystallographically distinct $Eu^{2+}$ sites present in the thin film.

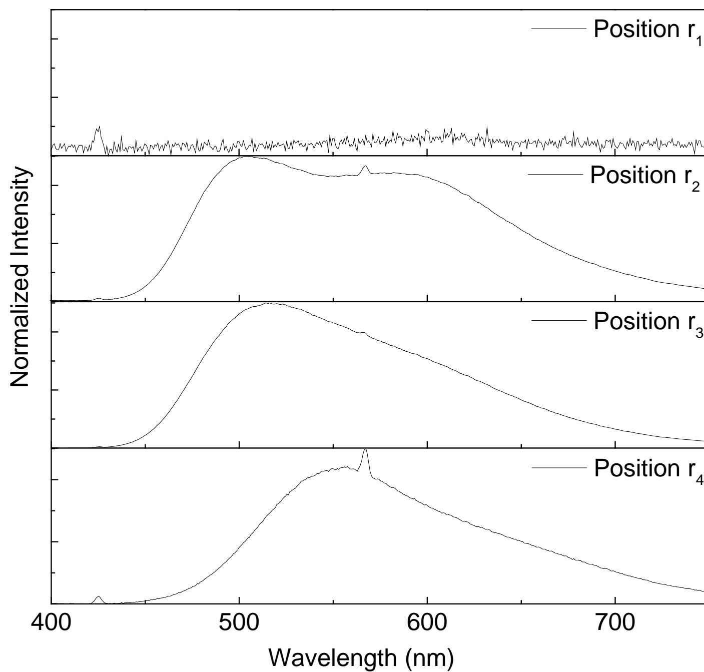


Fig. 6: Normalized emission spectra recorded at positions $r_1$-$r_4$.

By fitting a double Gauss function, two maxima were calculated at 500 nm and 580 nm at $r_2$. At $r_3$ primarily the band with the maximum at 500 nm is observed with the 580nm band as a low energy shoulder. This was confirmed by applying a double Gaussian fit. In the same way the emission band recorded at $r_4$ was found at 550 nm. The sharp low intensity peaks that are observed in the emission spectra at 420 nm 560 nm are second order scattered laser light (840/2 nm) from the higher harmonic

generator and third order laser light (280 nm) detected by the second order of the spectrometer grating (2x280 nm) that is reflected of the film surface, respectively.

The three PL bands that were observed are characteristic $Eu^{2+}$ $4f^{6}5d^{1} \rightarrow 4f^{7}$ emission bands. The $Eu^{2+}$ emission characteristic is well in agreement with the emission that is observed in $Eu^{2+}$ doped powders of the different crystalline oxynitride and oxide phases that were detected with XRD.

The black non-luminescent area around $r_1$ was found to be amorphous, with a very low intensity signal originating from $Ca_3Si_2O_4N_2$. Since no luminescence is present at this position, it is assumed that only a very small fraction of $Eu^{2+}$ doped $Ca_3Si_2O_4N_2$ is formed.

The green emission that is observed at $r_2$ originates from $Eu^{2+}$ doped $Ca_3Si_2O_4N_2$. A study on crystalline powders shows the same type of $Eu^{2+}$ emission band [5]. The host crystal has seven $Ca^{2+}$ sites that can be substituted by $Eu^{2+}$ ions. It was observed that by increasing the $Eu^{2+}$ doping concentration in the powders, the emission maximum shifts towards the red. By comparing the position of the emission maximum with the emission maximum that is reported here, it can be concluded that a 5% $Eu^{2+}$ doping concentration in the compounds is achieved. This is in good agreement with the values for the at% ratio of Ca to Eu of 1:20 that were measured with EDX (Fig. 4).

At $r_3$, the XRD pattern was found to match that of $Ca_2SiO_4$. The PL was identified in Fig. 6 as a broad band emission with a maximum at 500 nm. This characteristic $Eu^{2+}$ $4f^{6}5d^{1} \rightarrow 4f^{7}$ emission is typically observed in $Eu^{2+}$ doped $Ca_2SiO_4$ powder materials

[1-2]. Emission from the $CaSiO_3$ phase was not observed. This indicates that at $r_3$, an $Eu^{2+}$ doped $Ca_2SiO_4$ and a small fraction of $CaSiO_3$ are present.

The yellow light that was observed at $r_4$ consisting of broad band emission with a maximum at 550 nm is identical to $Eu^{2+}$ $4f^65d^1 \rightarrow 4f^7$ emission that was also observed in $Eu^{2+}$ doped $CaSiO_3$ powder materials [3]. This confirms that a luminescent $CaSiO_3:Eu^{2+}$ phase was formed at this position.

## 4. Discussion

The XRD, SEM, EDX and PL data consistently show that the oxidation process induces crystallization and activation of $Eu^{2+}$ luminescence of the as-deposited amorphous nitride film, consisting of $CaN_x$, $SiN_x$ and $EuN_x$. This process takes place in several stages in which first crystalline $Ca_3Si_2O_4N_2$, then $Ca_2SiO_4$ and finally $CaSiO_3$ is formed. Oxidation can be explained as the RTP system is not airtight. Therefore oxygen can diffuse into the $N_2/H_2$ gas flushed reactor chamber due to a low oxygen partial pressure. Oxidation starts on the top of the film and gradually progresses in lateral direction towards the silicon substrate. The oxidation rate and the final oxidation stage that is reached strongly depends on the position of the film.

A high oxidation rate is observed at the outer region of the film while almost no oxidation appears to take place at the center. The rate of an oxidation reaction is generally higher at elevated temperatures, so the formation of different oxides is most likely the result of the temperature gradient in the c-Si substrate during RTP treatment.

The heating and cooling rates at the edge are typically much higher than those in the center of the substrate during the ramp-up stage of the RTP. In the ramp-up stage this temperature variance can increase up to 150$^{o}$C in a double-sided illumination system such as the system that is used here [13]. During steady-state heating the temperature at the edge is 5-30$^{o}$C lower [13-17]. The oxidation rate of the film at the edge is therefore considered to be the highest during the ramp-up stage of the heating process. The rate of the oxidation reaction is lower in the other areas of the film, which oxidize primarily during the steady-state phase of the RTP treatments.

The different stages of the oxidation reaction are observed in Fig. 1. The emission color at the edge of the substrate changes with anneal time, as is observed throughout Fig. 1a-d. The emission colors are considered to originate from the different $Eu^{2+}$ doped oxynitride and oxide phases that were formed.

After the initial heat treatment of 10 minutes, $Eu^{2+}$ doped $Ca_3Si_2O_4N_2$ is formed at the edge of the film as is observed in Fig. 1b. This is the initial stage of the oxidation reaction. The formation of this greenish light emitting material is observed increasingly closer towards the center of the film (located at position $r_1$) as a function of anneal time. After 75 minutes of heating it is found closest to the center, which is designated as $r_2$ in Fig. 1d (r = 7 mm).

After 30 minutes of heat treatment, a bright white light emission is observed at the edge of the film (Fig. 1c). This emission originates from a $Ca_2SiO_4$:$Eu^{2+}$, which is the next stage of the oxidation reaction. The emission is also observed closer to the center of the film after longer annealing times and it is located at $r_3$ in Fig. 1d after 75 minutes of heating.

After 55 minutes of RTP treatment, the yellow light emitting phase was formed at the edge of the film, as is observed in Fig. 1c. The yellow light emitting $CaSiO_3:Eu^{2+}$ is the final stage of the oxidation reaction, since no more change was observed at the edge after 75 minutes of heating. The yellow light emitting area has expanded further towards the center of the film, as is observed in Fig. 1d where the area expands inward up to r = 18 mm, close to the location of $r_4$ (r = 23 mm). This shows that areas other than the edge of the film still oxidize after prolonged exposure to oxygen at high temperatures. It is therefore expected that by heating for a longer period of time, eventually the film will oxidize completely into crystalline $CaSiO_3$.

## 5. Conclusions

An experimental study was presented on the oxidation and crystallization process of thin films consisting of nitridated Ca, Si and Eu obtained by reactive magnetron sputtering. Heating at high ramp rates for a short time using a double-sided illumination RTP system resulted in the formation of crystalline $Eu^{2+}$ doped luminescent $Ca_3Si_2O_4N_2:Eu^{2+}$ oxy-nitride thin-films.

After a prolonged heat treatment crystalline $Ca_2SiO_4:Eu^{2+}$ and finally $CaSiO_3:Eu^{2+}$ is formed. This step-wise oxidation reaction is initiated at the surface of the film and progresses in lateral direction towards the Si-substrate, generating an oxide layer on top of a nitride layer. The oxidation rate was found to be higher at the edge of the substrate due to a radial temperature gradient in the c-Si substrate during the temperature ramp-up phase of the RTP.

Reactive magnetron sputtering proves to be an adequate technique for deposition of nitridated Ca, Si and Eu thin films. This work shows that provided full control of oxygen content and temperature gradient can be obtained, single phase luminescent oxynitride or even nitride films might be obtained. To obtain such control, RTP systems with controlled inflow of $N_2/H_2$ gas in an oxygen-free atmosphere need to be used.

**Acknowledgements**

Ruud Hendrikx at the Department of Materials Science and Engineering of the Delft University of Technology is acknowledged for the X-ray analysis. Financial support is acknowledged for this research from ADEM, A green Deal in Energy Materials of the Ministry of Economic Affairs of The Netherlands.

**References**

[1] Y.Y. Luo, D.S. Jo, K. Senthil, S. Tezuka, M. Kakihana, K. Toda, T. Masaki, D.H. Yoon, Synthesis of high efficient $Ca_2SiO_4:Eu^{2+}$ green emitting phosphor by a liquid phase precursor method, J. Sol. State Chem. 189 (2012) 68.

[2] S. Choi, S. Hong, Characterization of $Ca_2SiO_4:Eu^{2+}$ Phosphors Synthesized by Polymeric Precursor Process, J. Am. Ceram. Soc. 92 (2009) 2025.

[3] S. Ye, X. Wang and X. Jing, Energy Transfer among $Ce^{3+}$, $Eu^{2+}$, and $Mn^{2+}$ in $CaSiO_3$, J. Electroc. Soc. 155 (2008) J143.

[4] R. Xie, N. Hirosaki, Silicon-based oxynitride and nitride phosphors for white LEDs—A review, Sci. Tech. Adv. Mater. 8 (2007) 588.

[5] Y. Chiu, C. Huang, T. Lee, W. Liu, Y. Yeh, S. Jang, R. Liu, $Eu^{2+}$-activated silicon-oxynitride $Ca_3Si_2O_4N_2$: a green-emitting phosphor for white LEDs, Optics Express 19 (2011) A331.

[6] X. Song, R. Fu, S. Agathopoulos, H. He, X. Zhao et al. Photoluminescence properties of $Eu^{2+}$-activated $CaSi_2O_2N_2$: Redshift and concentration quenching, J. Appl. Phys. 106 (2009) 033013.

[7] Y.Q. Li, J.E.J. van Steen, J.W.H. van Krevel, G. Botty, A.C.A. Delsing, F.J. DiSalvo, G. de With, H.T. Hintzen, Luminescence properties of red-emitting $M_2Si_5N_8:Eu^{2+}$ (M = Ca, Sr, Ba) LED conversion phosphors, J. All. Comp. 417 (2006) 273.

[8] B.S. Richards, Enhancing the performance of silicon solar cells via the application of passive luminescence conversion layers, Sol. Energy Mater. Sol. Cells 90 (2006) 2329.

[9] T. Trupke, M.A. Green, P. Würfel, Improving solar cell efficiencies by down-conversion of high-energy photons, J. Appl. Phys. 92 (2002) 1668.

[10] V. Badescu, A. de Vos, A.M. Badescu, A. Szymanska, Improved model for solar cells with down-conversion and down-shifting of high-energy photons. J. Phys. D: Appl. Phys. 40 (2007) 341.

[11] O.M. ten Kate, M. de Jong, H.T. Hintzen, E. van der Kolk, Efficiency enhancement calculations of state-of-the-art solar cells by luminescent layers with spectral shifting, quantum cutting and quantum tripling function, J. Appl. Phys. 114 (2013) 084502.

[12] M. de Jong, V.E. van Enter, E. van der Kolk, DC/RF magnetron sputter deposition and characterisation of $Ca_3Si_2N_2O_4:Eu^{2+}$ luminescent thin films, J. Lumin. *under review* (2015).

[13] J.P. Hebb, K.F. Jensen, The Effect of Patterns on Thermal Stress During Rapid Thermal Processing of Silicon Wafers, IEEE Transactions on Semiconductor Manufacturing 11 (1998) 99-107.

[14] W.S. Yoo, T. Fukada, I. Yokoyama, K. Kang, N. Takahasi, Thermal Behavior of Large-Diameter Silicon Wafers during High-Temperature Rapid Thermal Processing in Single Wafer Furnace, Jpn. J. Appl. Phys. 41 (2002) 4442-4449.

[15] B.K. Tanner, J. Wittge, D. Allen, M.C. Fossati, A.N. Daniwesky, P. McNally, J. Garagorri, M.R. Elizalde, D. Jacques, Thermal slip sources at the extremity and bevel edge of silicon wafers, J. Appl. Cryst. 44 (2011) 489-494.

[16] M.M. Moslehi, Process Uniformity and Slip Deformation Patterns in Linearly Ramped-Temperature Transient Rapid Thermal Processing of Silicon, IEEE Transactions on Semiconductor Manufacturing 2 (1989) 130-141.

[17] C. Schaper, Y. Cho, P. Park, S. Norman, P. Gyugyi, G. Hoffmann, S. Balemi, S. Boyd, G. Franklin, T. Kailath and K. Saraswat, Modeling and Control of Rapid Thermal Processing, SPIE Proceedings of Rapid Thermal Processing (1991).

**ECN**

Westerduinweg 3
1755 LE Petten
The Netherlands

P.O. Box 1
1755 LG Petten
The Netherlands

T +31 88 515 4949
F +31 88 515 8338
info@ ecn.nl
www.ecn.nl